Energy & Environmental Science

ROYAL SOCIETY OF CHEMISTRY

PAPER

View Article Online
View Journal | View Issue

Cite this: *Energy Environ. Sci.*, 2025, **18**, 6587

Improved efficiency and stability of outdoor and indoor organic photovoltaics with suppressed voltage loss *via* alkoxylation on dimeric giant acceptors featured as supramolecular stabilizers†

Ho Ming Ng,‡[ab] Bosen Zou,‡[ab] Aleksandr Sergeev,[c] Yuang Fu,[d] Pok Fung Chan,[d] Zefan Yao,[e] Qingyuan Wang,[f] Zhengkai Li,[f] Chun-Jen Su,[g] U-Ser Jeng,[g] Xiaotian Hu,[h] Gang Li,[a] Xinhui Lu,[d] Kam Sing Wong,[c] Zhi-Guo Zhang,[f] Yiwang Chen,[h] Wai-Yeung Wong,*[a] Han Yu*[ab] and He Yan*[b]

Organic solar cells (OSCs) have shown remarkable progress in power conversion efficiencies (PCEs), largely driven by the development of small-molecule acceptors (SMAs), with PCEs of over 20%. However, their stability issue has become a critical factor that limits the commercialization of SMA-OSCs. Therefore, we developed a novel dimeric giant acceptor (DGA), named DYO-V, featuring alkoxy chains on the β-position of the outer thienothiophen, with upshifted energy levels for suppressed voltage losses. By connecting with one vinylene linker, DYO-V demonstrated a rigid and co-planar conformation, leading to a high binding energy with a high glass transition temperature for stable morphology. This DGA supramolecular stabilizer exhibited complementary absorption, durable morphology and photon dynamics to simultaneously achieve high efficiency and stability in ternary devices. Therefore, the fabricated PM6:BTP-eC9:DYO-V device achieved a PCE of 20.2%, which represents the highest PCE achieved for DGA-based OSCs with a high open-circuit voltage (V_{OC}) of 0.90 V and robust device stability (T_{90} = 2000 hours). Furthermore, the hypsochromic DYO-V exhibited excellent indoor photovoltaic performance with a PCE of 28.1% for PM6:DYO-V, which is the best performance observed for DGA-indoor organic photovoltaics. Thus, this work presents an effective strategy for designing DGAs with wider bandgaps for efficient and stable outdoor and indoor photovoltaic applications.

Received 5th February 2025,
Accepted 7th April 2025

DOI: 10.1039/d5ee00668f

rsc.li/ees

Broader context

Organic solar cells (OSCs) have rapidly advanced in efficiency; however their long-term stability remains a key challenge for their commercialization. The introduction of dimeric giant acceptors (DGAs) represents a significant breakthrough in addressing this limitation, offering enhanced morphological stability and improved charge transport. Our study presents DYO-V, a novel DGA featuring alkoxy side chains and a vinylene linkage, which effectively fine-tunes energy levels, suppresses voltage losses, and strengthens device robustness. With a record-breaking PCE of 20.2% for DGA-based OSCs and an exceptional efficiency of 28.1% under indoor lighting, DYO-V demonstrates the potential of DGAs in both outdoor and indoor photovoltaics. This work not only advances the fundamental understanding of DGA-based OSCs but also paves the way for their practical deployment in diverse energy-harvesting scenarios. By addressing both efficiency and stability issues, our findings contribute to the realization of OSCs as viable and sustainable alternatives for next-generation energy solutions, supporting the global transition toward renewable energy and carbon neutrality.

[a] *Department of Applied Biology and Chemical Technology and Research Institute for Smart Energy, The Hong Kong Polytechnic University, Hung Hom, 999077, Hong Kong. E-mail: wai-yeung.wong@polyu.edu.hk, yuhan.yu@polyu.edu.hk*
[b] *Department of Chemistry and Hong Kong Branch of Chinese National Engineering Research Center for Tissue Restoration and Reconstruction, The Hong Kong University of Science and Technology, Clear Water Bay, Kowloon, Hong Kong 999077. E-mail: hyan@ust.hk*
[c] *Department of Physics, The Hong Kong University of Science and Technology, Clear Water Bay, Kowloon, Hong Kong 999077*
[d] *Department of Physics, Chinese University of Hong Kong, New Territories, Hong Kong 999077*
[e] *College of Chemistry and Molecular Engineering, Peking University, Beijing 100871, China*
[f] *State Key Laboratory of Chemical Resource Engineering, Beijing Advanced Innovation Center for Soft Matter Science and Engineering, Beijing University of Chemical Technology, Beijing 100029, China*
[g] *National Synchrotron Radiation Research Center, 101 Hsin-Ann Road, Science-Based Industrial Park, Hsinchu 300092, Taiwan*
[h] *College of Chemistry and Chemical Engineering/Film Energy Chemistry for Jiangxi Provincial Key Laboratory (FEC), Nanchang University, Nanchang, China*

† Electronic supplementary information (ESI) available. See DOI: https://doi.org/10.1039/d5ee00668f

‡ H. M. Ng and B. Zou contributed equally to this work.

Introduction

Organic solar cells (OSCs) have experienced great success under the convoy of small molecule acceptors (SMAs), promoting power conversion efficiencies (PCEs) of over 20%.[1–7] However, the challenge of SMA-OSCs lies in simultaneously enhancing the device efficiency and operational stability. The lack of stability predominantly stems from the *meta*-stable morphology, where the optimum active layer is not at the thermodynamic state with the lowest energy after thermal annealing. The SMAs with high diffusion coefficients[8–11] are kinetically unstable against morphology diffusion and tend to self-aggregate into small-scale isolated domains under external stress and thermodynamic restrictions,[12,13] causing burn-in degradation.[14–16] Conversely, long-term stability is influenced more by the continuous degradation of both the active layer and charge transport layers, driven by photo-oxidation and UV-induced bond breaking upon light exposure. To overcome this, dimeric giant acceptor (DGA)-based OSCs, adopting acceptors with high and accurate molecular weight, have emerged as an effective strategy to simultaneously balance the device efficiency and stability by offering comparable crystallinity to SMAs for charge transport and providing a supramolecular structure with a high glass transition temperature (T_g), slow diffusion rates and excellent stability.[10,17–20] Benefitting from the development of the Y-series DGAs, the PCEs of DGA-OSCs have surpassed 19%.[19,21]

To further optimize the efficiency and stability of OSCs, the ternary tactic is considered an effective strategy that introduces a DGA as the third component into the binary SMA-OSC systems, as they provide an optimal balance between the crystallization and material robustness for trade-off between efficiencies and stability.[22–29] In our previous report, the highly crystalline small-molecule acceptor Y6-O[30] tended to aggregate into large domains after long-term operation, potentially disrupting the film morphology, and thereby resulting in inferior device stability. In contrast, the high molecular weight polymer acceptor (PYO-V) could maintain excellent device stability. However, the efficiency enhancement was not significant owing to the weaker crystallinity of the polymer acceptors. DGAs, with similar structures but larger molecule weights than SMAs in the host, could strengthen the morphology by slowing diffusion to enhance the device robustness, while maintaining excellent crystallinity. Despite this, most reported Y-series DGAs exhibit overlapping absorption and comparable energy levels, which conflicts with the principle of complementary absorption and suppressed voltage loss for maximizing the ternary device performance.[31–33] Introducing alkoxy side chains at the β-position of the outer thiophene in Y-series SMAs and polymer acceptors has proven to be an effective strategy for blue-shifting the absorption and up-shifting the LUMO levels, owing to the weakened intramolecular charge transfer (ICT) effect.[30,34–36] Benefiting from the panchromatic absorption and suppressed voltage loss, alkoxy acceptors serve as highly effective components for optimizing ternary devices.[37,38] Moreover, the intramolecular conformational locking of alkoxy chains and vinylene linkage can also be applied to construct a rigid backbone to suppress non-radiative voltage loss and facilitate molecular packing for better morphology stability.[37,39] In addition to outdoor applications, the alkoxy acceptors developed by our team demonstrate overlapping absorption with light-emitting-diode (LED) light sources,[40–43] making them promising for indoor photovoltaics.[44,45] Given the non-toxic and eco-friendly nature of indoor organic photovoltaics, it is regarded as a sustainable power source for low-energy devices in smart homes and Internet of Things (IoT) systems.[46] Therefore, alkoxylation on DGAs is anticipated to further enhance the efficiency and stability of outdoor and indoor photovoltaics.

To investigate the alkoxy effect on Y-series DGAs for versatile OSC applications, we designed and synthesized a DGA, named DYO-V, with alkoxy side chains on the thiophene moiety of the classical Y-series monomers connected by one vinylene linker (Fig. 1). Theoretical calculations revealed the rigid and co-planar conformation of DYO-V. Thus, both higher binding energy and higher T_g are achieved for slow diffusion rates and stable morphology. Simultaneously, the alkoxy DYO-V exhibits blue-shifted absorption and up-shifted energy levels compared to the classical Y-series acceptors, providing complementary absorption as guest acceptors with the host of PM6:BTP-eC9, and effectively suppresses the voltage loss. Therefore, the PM6:BTP-eC9:DYO-V ternary devices achieved a high open-circuit voltage (V_{OC}) of 0.90 V, a short-circuit current (J_{SC}) of 28.0 mA cm^{-2}, and an impressive PCE of 20.2%, which is much higher than that of PM6:BTP-eC9 devices (18.8%), exhibiting the best efficiency of DGA-based OSCs (Table S1, ESI†). Furthermore, the morphology and photophysical dynamics of the ternary blend demonstrated a stronger crystallinity and ideal phase segregation with 30 wt% DYO-V, thus boosting efficient exciton dissociation, rapid charge transport and suppressed charge recombination. Based on these advantages, the ternary devices suggest a remarkable device stability with a T_{90} of 2000 hours. In addition to the outdoor photovoltaics under one-sun illumination, DYO-V also performs as an efficient and stable indoor photovoltaic material in binary devices under LED illumination for versatile photovoltaics, delivering an inspiring efficiency of 28.1% with 2600 K LED light, which is among the best performance for indoor DGA-OSCs. This work demonstrates an effective strategy of alkoxy side chains for tuning the optoelectrical and crystallinity properties of DGAs, and for achieving efficient and stable OSCs for outdoor and indoor photovoltaic applications.

Results and discussion

Material design and optoelectrical properties

The chemical structures of PM6, BTP-eC9 and DYO-V are presented in Fig. 1(a). The synthesis details and characterization data of the DYO-V, including nuclear magnetic resonance and mass spectra, are summarized in the ESI† (Scheme S1 and Fig. S1, S2). Density functional theory (DFT) calculations revealed that the dihedral angles between the end groups and the central backbone is reduced to 3.93° after side chain alkoxylation (Fig. S3, ESI†), which is attributed to the intramolecular locking effect caused by the oxygen-assisted non-covalent interaction, thus benefitting the

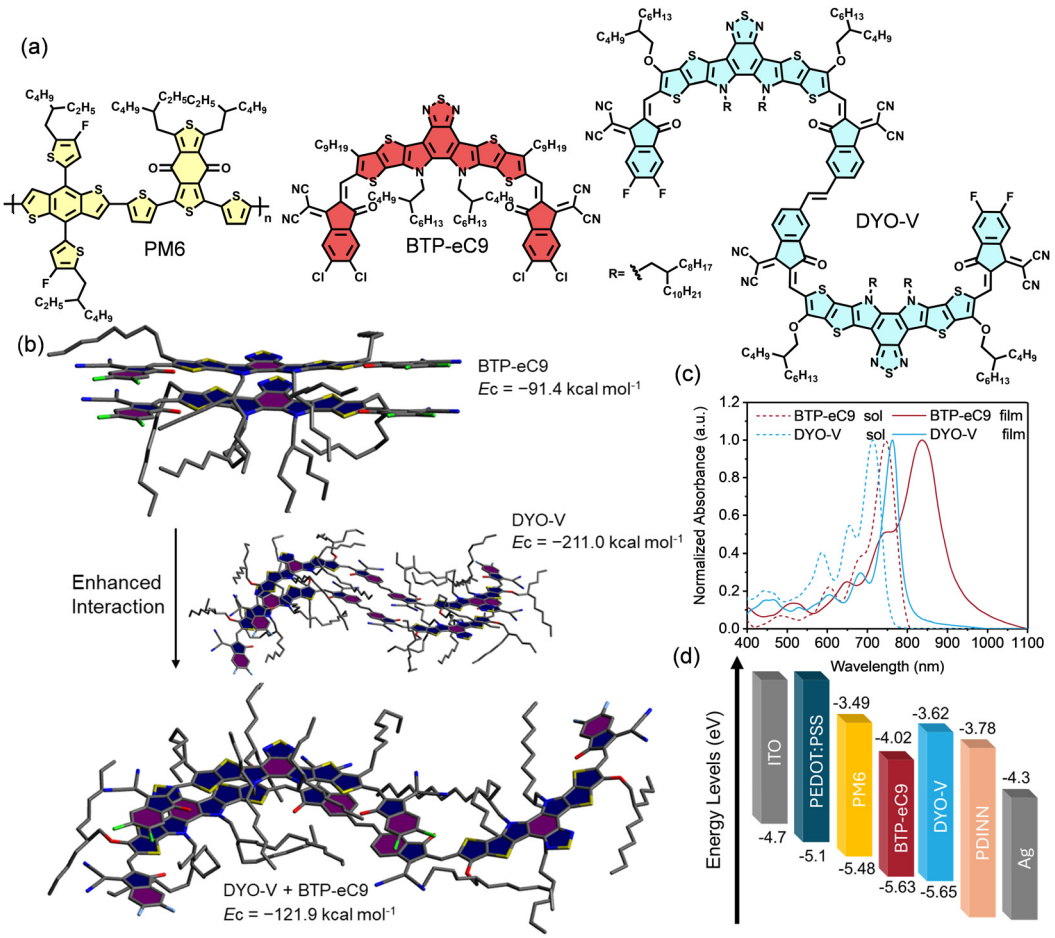

Fig. 1 (a) Chemical structures of PM6, BTP-eC9 and DYO-V. (b) Non-covalent interaction energies of BTP-eC9/BTP-eC9, DYO-V/DYO-V and BTP-eC9/DYO-V obtained from MD simulations and DFT calculations. (c) Normalized UV-Vis absorption spectra of the BTP-eC9 and DYO-V in the chloroform solution and the neat film state. (d) Energy alignment of the materials and device structure in OSCs.

molecular packing.[47,48] Molecular dynamics (MD) simulations were carried out to generate the stable interacting molecules, which are sorted by energy, and were further optimized at the GFN2-xTB level of theory.[49] DFT calculations at the B3LYP-D3BJ/def2-SVP level were further performed in the ORCA package to elucidate the interaction energies of BTP-eC9/BTP-eC9, DYO-V/DYO-V and BTP-eC9/DYO-V,[50–52] which are summarized in Fig. 1(b). As a result, the largest non-covalent interaction energy between DYO-V delivers a complexation energy (E_c) = −211.0 kcal mol^{-1}. Most importantly, the E_c between DYO-V and BTP-eC9 is strengthened to −121.9 kcal mol^{-1}, in comparison to that of BTP-eC9/BTP-eC9 (−91.4 kcal mol^{-1}). This enhanced interaction energy could impede BTP-eC9 agglomeration in ternary films for optimized and stabilized morphology.

The normalized solution-state ultraviolet-visible (UV-Vis) absorption spectra are displayed in Fig. 1(c). DYO-V exhibits a maximum absorption peak ($\lambda_{max,sol}$) at 714 nm with a significant blue-shift compared to the classical BTP-eC9 ($\lambda_{max,sol}$ = 746 nm), which is attributed to the weaker ICT effect of alkoxy substitution. In thin-film states, the $\lambda_{max,film}$s of DYO-V and BTP-eC9 are red-shifted to 762 nm and 837 nm, respectively, corresponding to optical bandgaps (E_gs) of 1.53 eV and 1.33 eV. Apart from absorption, steady-state photoluminescence spectra were measured to investigate the conformational rigidity of the materials through the determined Stokes shifts (Fig. S4, ESI†). DYO-V exhibits a smaller Stokes shift of 38 nm than BTP-eC9 (72 nm), demonstrating a rigid skeleton and smaller energetic disorder, which is expected to suppress the non-radiative voltage loss in devices.[53] In terms of electrochemical properties, both DFT calculations (Fig. S5, ESI†) and cyclic voltammetry (CV) confirm the larger bandgap and up-shifted LUMO level of DYO-V. The CV results (Fig. S6, ESI†) revealed the LUMO/HOMO energy levels to be −3.62/−5.65 eV for DYO-V and −4.02/−5.63 eV for BTP-eC9. This is due to the electron-donating effect of the alkoxy chains on the end groups. Thus, the decreased ICT leads to a blue-shifted absorption and higher energy levels relative to the classical SMAs.[30,34] Therefore, DYO-V demonstrates great potential as a guest component to complement the absorption and minimize the voltage loss for better ternary devices.

Thermal transition analysis

The thermal phase transition of the BTP-eC9 and DYO-V is employed to evaluate their resistance to morphological

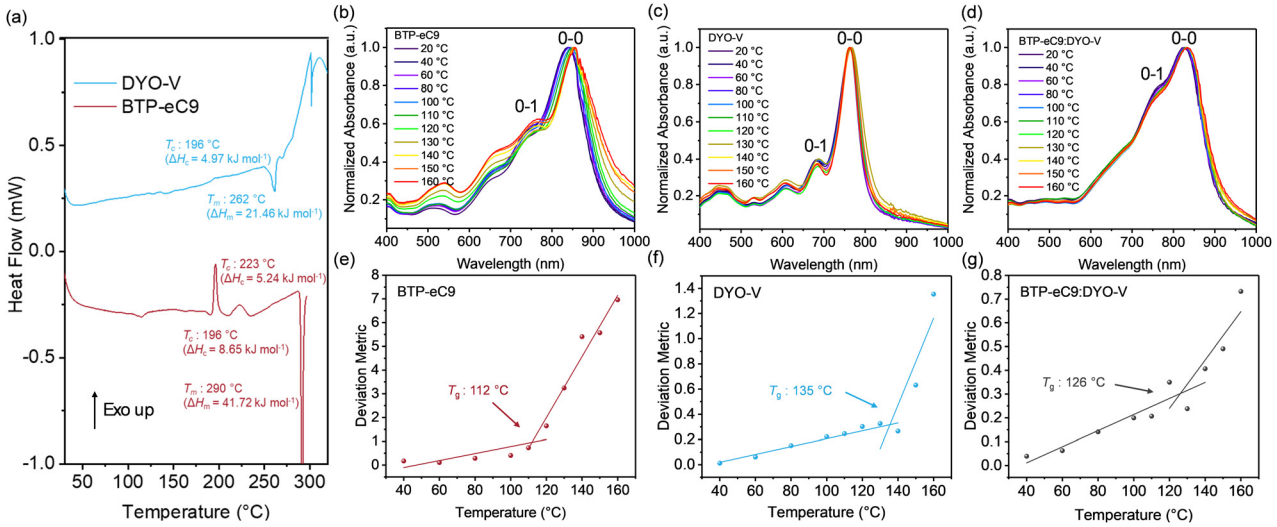

Fig. 2 (a) DSC thermograms of BTP-eC9 and DYO-V, collected from the first cycle with a 10 °C min^{-1} heating rate. (b)–(d) Temperature-dependent absorption spectra and (e)–(g) deviation metrics obtained from the temperature-dependent absorption of the BTP-eC9, DYO-V and BTP-eC9:DYO-V films.

diffusion under thermal stress, which directly impacts the stability of OSCs. Differential scanning calorimetry (DSC) measurements were performed to investigate the phase transition properties, including molecular diffusion, nucleation rate and crystallization kinetics.[54] As shown in Fig. 2(a), both lower crystallization enthalpy (ΔH_c) and melting enthalpy (ΔH_m) of DYO-V demonstrate its less energetically favourable crystallization process relative to BTP-eC9. Despite their similar exothermal cold crystallization temperatures (T_cs) at 196 °C, BTP-eC9 shows a sharp transition peak that is indicative of a faster crystallization process, while DYO-V exhibits a broad T_c peak, suggesting that the supramolecular character could hinder the crystal growth. Temperature-dependent absorption measurements (Fig. 2(b)–(g)) were used to determine the material's T_g values for the thermal phase transitions.[55] The T_g values for BTP-eC9, DYO-V and BTP-eC9:DYO-V are 112 °C, 135 °C and 126 °C, respectively. Besides the T_g, BTP-eC9 shows an increasing ratio of the 0–0/0–1 peaks with increasing temperature (Fig. 2(b)), indicating a phase rearrangement from J- to H-aggregation.[56] Benefiting from the supramolecular character of DYO-V, BTP-eC9:DYO-V suppresses this phase transition with an increased T_g of 126 °C, as well as a reduced 0-1 peak (Fig. 2(d)), which will promote the ternary device stability after introducing the supramolecular stabilizer DYO-V.

Outdoor photovoltaic performance

To study the alkoxy DGA effect on device efficiency and stability, devices were fabricated using the conventional device structure of ITO/PEDOT:PSS/active layer/PNDIT-F3N/Ag. PM6 was chosen as the donor for its high performance and universality in OSCs. The *J*–*V* curves are depicted in Fig. 3(a), and the device parameters are summarized in Table 1. Benefiting from the higher LUMO level of DYO-V, the PM6:DYO-V device exhibits an extremely high V_{OC} of 1.005 V relative to the 0.852 V of the PM6:BTP-eC9 counterpart devices. Despite that, the narrower photon harvesting extent of DYO-V results in a diminished J_{SC}, leading to a PCE of 16.3%. Interestingly, when incorporating DYO-V as the guest component into the PM6:BTP-eC9 host, the ternary device achieved a significantly enhanced V_{OC} of 0.897 V compared to the binary PM6:BTP-eC9 (0.852 V), together with overall enhancements in J_{SC} (27.3 mA cm^{-2}) and FF (80.4%). Both improved V_{OC} and J_{SC} are attributed to the up-shifted LUMO and complementary absorption of DYO-V. As a result, the PM6:BTP-eC9:DYO-V ternary device delivers a champion PCE of 20.2%, which is the best performance for DGA-based OSCs (Fig. 3(b)).

External quantum efficiency (EQE) measurements (Fig. 3(c)) further support these findings, where the ternary device exhibits a higher photo-response across the whole photon-harvesting range relative to the binary BTP-eC9 host. In addition to the efficiency, the operational device stability was evaluated in N_2 atmosphere under 65 °C and LED light to assess the thermal stability. PM6:DYO-V demonstrates burn-in degradation-free behaviour. This is attributed to the robust morphology maintained by the DGA with a high T_g. In contrast, PM6:BTP-eC9 experienced severe burn-in degradation invoked by the rapid molecular diffusion of BTP-eC9 with a lower T_g. Interestingly, a slower degradation is observed for PM6:BTP-eC9 after thermal stability for 1800 h. This could be attributed to the morphology reaching a *meta*-thermodynamically stable equilibrium state. Furthermore, the incorporation of DYO-V into the binary host can also reduce both burn-in and long-term continuous degradation (Fig. 3(d)), which proves that our alkoxy DGA is an effective strategy for OSCs with improved stability.

Voltage loss (V_{loss}) analysis was conducted to investigate the origin of the higher V_{OC} in DYO-V-based devices, and is summarized in Fig. 3(e) and Table S2 (ESI†). The E_g values of the devices were determined through dual fitting of the EQE and electroluminescence spectra (Fig. S7, ESI†). The total V_{loss} values for PM6:BTP-eC9, PM6:DYO-V and PM6:BTP-eC9:DYO-V were

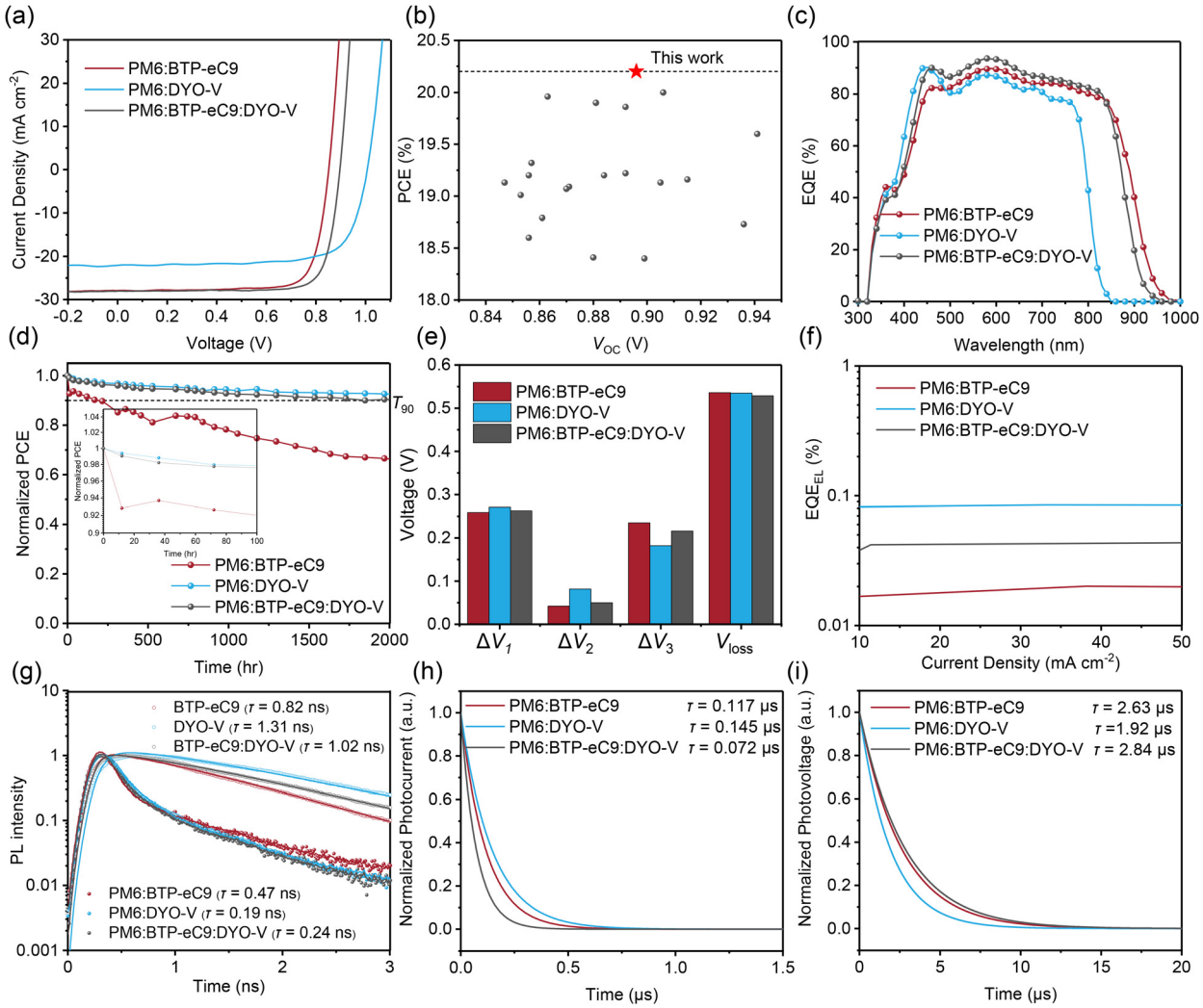

Fig. 3 (a) J–V characteristics of the devices. (b) Summary of the representative DGA-based OSCs and PM6:BTP-eC9:DYO-V in V_{OC} vs PCE. (c) External quantum efficiency (EQE) spectra and (d) thermal stability of the devices. (e) Voltage loss profile, (f) EQE$_{EL}$ spectra of the devices. (g) Time-resolved photoluminescence (TRPL) of the pristine and blend of BTP-eC9, DYO-V and BTP-eC9:DYO-V; the pump and probe wavelengths are 790 and 860 nm, respectively. (h) Transient photocurrent (TPC) and (i) transient photovoltage (TPV) of the PM6:BTP-eC9, PM6:DYO-V and PM6:BTP-eC9:DYO-V devices.

Table 1 Photovoltaic parameters of the PM6:BTP-eC9, PM6:DYO-V and PM6:BTP-eC9:DYO-V under an AM 1.5 G illumination intensity of 100 mW cm^{-2}

Materials	V_{OC} [V]	J_{SC} [mA cm^{-2}]	J_{cal} [mA cm^{-2}]	FF [%]	PCE^a [%]
PM6 : BTP-eC9 (1 : 1.2)	0.852 (0.850 ± 0.003)	27.9 (27.7 ± 0.2)	27.1	79.1 (78.9 ± 0.3)	18.8 (18.6 ± 0.2)
PM6 : DYO-V (1 : 1.2)	1.005 (1.004 ± 0.002)	22.0 (21.9 ± 0.2)	22.0	73.6 (73.4 ± 0.2)	16.3 (16.1 ± 0.2)
PM6 : BTP:ec9 : DYO-V (1 : 0.8 : 0.4)	0.897 (0.896 ± 0.002)	28.0 (27.8 ± 0.3)	27.3	80.4 (80.1 ± 0.3)	20.2 (19.9 ± 0.3)

^{a} Average values from 15 devices with the deviation shown in parentheses.

found to be 0.536, 0.535 and 0.523 V, respectively. To confirm that the rigid alkoxy DGA was responsible for the suppressed non-radiative recombination, the electroluminescence quantum efficiency (EQE$_{EL}$) was measured. As shown in Fig. 3(f), the PM6:DYO-V device achieves the highest EQE$_{EL}$ of 8.8 × 10^{-4}, followed by PM6:BTP-eC9:DYO-V and PM6:BTP-eC9 with EQE$_{EL}$ values of 2.4 × 10^{-4} and 1.1 × 10^{-4}, respectively, corresponding to the non-radiative recombination voltage losses (ΔV_3) of 0.182, 0.216 and 0.235 V. The minimized ΔV_3 of PM6:BTP-eC9:DYO-V is attributed to the decreased number of vibrational states and recombination channels introduced by the alkoxy side chains; therefore, a dramatically enhanced V_{OC} is realized in the ternary device, as shown above.

Time-resolved photoluminescence (TRPL) measurements of the pure and blend films were employed to study the exciton dissociation process (Fig. 3(g)). Under excitation at 790 nm, the pure BTP-eC9 presented a PL decay lifetime of 0.82 ns, which decreased to 0.47 ns when blending with PM6, illustrating an

effective hole transfer from the acceptor to the donor. Upon introducing the DGA DYO-V as the third component, the PL quenching process accelerates to 0.24 ns, suggesting a faster exciton dissociation promoted by the DYO-V addition. The larger exciton dissociation probability ($P(E,T)$) of PM6:BTP-eC9:DYO-V also exhibits a higher extent of exciton dissociation (Fig. S8, ESI†). The detailed excited-state dynamics will be investigated through transient absorption technology (*vide infra*).

Transient photocurrent (TPC) and the transient photovoltage (TPV) measurements were conducted to explore the charge extraction and recombination process (Fig. 3(h) and (i)). The photocurrent decay times for PM6:BTP-eC9, PM6:DYO-V and PM6:BTP-eC9:DYO-V are 0.117 μs, 0.145 μs and 0.072 μs, respectively, while the photovoltage decay times are 2.63 μs, 1.92 μs and 2.84 μs. These results indicate both faster charge extraction and longer carrier lifetimes for ternary devices, correlating with their improved FFs. Moreover, light-intensity-dependent V_{OC}/J_{SC} experiments (Fig. S9, ESI†) further reveal that ternary devices suffered from the lowest extent of the bimolecular/trap-assisted recombination process. Hole/electron mobilities (μ_h/μ_e) were calculated using the space-charge-limited-current (SCLC) method (Fig. S10 and Table S3, ESI†). PM6:DYO-V displays an inferior μ_h of 4.3×10^{-4} cm^2 V^{-1} s^{-1} when blended with PM6. However, the incorporation of DYO-V improves the μ_h/μ_e of BTP-eC9 binary devices from ($4.9/5.4 \times 10^{-4}$ cm^2 V^{-1} s^{-1}) to ($5.4/5.7 \times 10^{-4}$ cm^2 V^{-1} s^{-1}), resulting in a more balanced μ_h/μ_e ratio and thus ensuring the higher FF.

Morphology stability characterization

DGAs have the most crucial impact on the morphology stability, which is necessary to investigate the origin of the device stabilities. Grazing incidence wide angle X-ray scattering (GIWAXS) measurements were employed to characterize the molecular packing in fresh and aged samples (Fig. 4(a) and Tables S4, S5, ESI†). For fresh blends, PM6:BTP-eC9:DYO-V exhibits a smaller π–π stacking distance of 3.61 Å and a larger crystal coherence length (CCL) of 29.3 Å. This is indicative of stronger crystallinity after mixing the DYO-V into the host, which is due to the larger binding energy of DYO-V, as calculated. After thermal aging at 120 °C for 36 hours, the binary PM6:BTP-eC9 exhibits reduced π–π stacking peak intensity with an increased CCL. This indicates crystal growth driven by D:A phase segregation, which is attributed to the high diffusion coefficient of the BTP-eC9 SMA, as evidenced by its low T_g. In contrast, the morphology of the ternary blend remains identical with no discernible differences in the GIWAXS patterns after thermal aging, indicating the higher T_g of the DYO-V with suppressed molecular diffusion. Moreover, the surface morphology through atomic force microscopy (AFM, Fig. S11, ESI†) also demonstrated a similar trend, in which the aged PM6:BTP-eC9 blend suffers from noticeable agglomerations along with an increased root-mean-square (RMS) surface roughness from 1.12 nm to 1.45 nm relative to the DYO-V-based blends with negligible changes.

As for the phase segregation, grazing-incidence small-angle X-ray scattering (GISAXS) measurements were utilized to display the variation. The analysis of $2R_{gc}$ (crystalline domain size) and D_f (fractal dimension) are summarized in Fig. 4(h)–(j) and Table S6 (ESI†). The ternary PM6:BTP-eC9:DYO-V suggests a smaller $2R_{gc}$ (34.0 nm) than that of PM6:BTP-eC9 (35.4 nm), thus benefitting the exciton dissociation, suppressed recombination and a higher FF in ternary devices. After thermal aging,

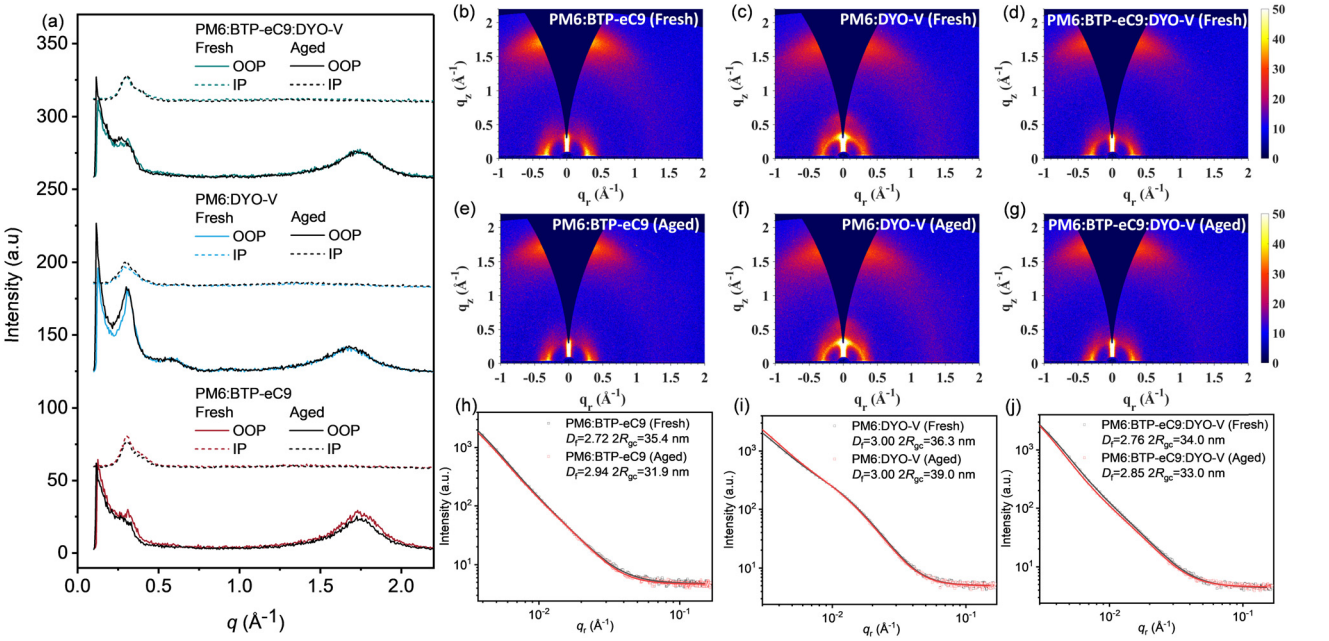

Fig. 4 (a) 1-D GIWAXS line-cuts along the in-plane (IP) and out-of-plane (OOP) directions for fresh and aged blend films. 2D GIWAXS plots of the PM6:BTP-eC9, PM6:DYO-V and PM6:BTP-eC9:DYO-V (b)–(d) fresh and (e)–(g) aged samples. (h)–(j) Corresponding in-plane GISAXS line-cuts of the fresh and aged blend films.

the $2R_{gc}$ of PM6:BTP-eC9 decreases from 35.4 to 31.9 nm along with an increase in the D_f from 2.72 to 2.94. A higher D_f indicates the formation of more agglomerated domains with less inter-domain connectivity, potentially leading to isolated acceptor phases that can trap electrons.[57] In contrast, the incorporation of DYO-V in the ternary device can effectively mitigate this densification, resulting in a comparable D_f without notable changes in $2R_{gc}$ (Fig. 4(j)), originating from the durable phase segregation of the binary PM6:DYO-V (Fig. 4(i)). Based on the above morphology results, the DGA with a larger binding energy and slow diffusion rates not only effectively optimized the morphology but also maintained the robust stability for long-term operation.

Photophysical dynamics study

To investigate the photophysical dynamics in detail, transient absorption (TA) spectroscopy was performed on the pristine (Fig. S12, ESI†) and blend (Fig. 5(a)–(c)) films under selective excitation of DYO-V at 750 nm and BTP-eC9 at 790 nm (Fig. S13, ESI†), respectively, while both wavelengths were used for the BTP-eC9:DYO-V blends. Using the MCR-ALS decomposition described in a previous study,[58] the datasets of neat acceptors and their blends with PM6 were decomposed into time and spectral components. Two components corresponded to LE (Fig. S14, ESI†). Furthermore, the delocalized exciton (DE) states (Fig. S15, ESI†) are dominant in the TA signal from the acceptor domains. There is also a distinct positive $\Delta T/T$ signal in the 580–680 nm range, corresponding to the ground-state bleaching of the donor. The decomposed spectral and time components of the BTP-eC9 and BTP-eC9:DYO-V films (Fig. S14a, ESI†) appear to be highly similar, with minor DYO-V's LE contributions observed in BTP-eC9:DYO-V (Fig. S14b, ESI†), indicating that the LE states in BTP-eC9:DYO-V originate primarily from the BTP-eC9 domain. Additionally, DYO-V's LE states show significantly faster TA kinetics in BTP-eC9:DYO-V compared to the DYO-V neat films (Fig. S14d, ESI†), suggesting

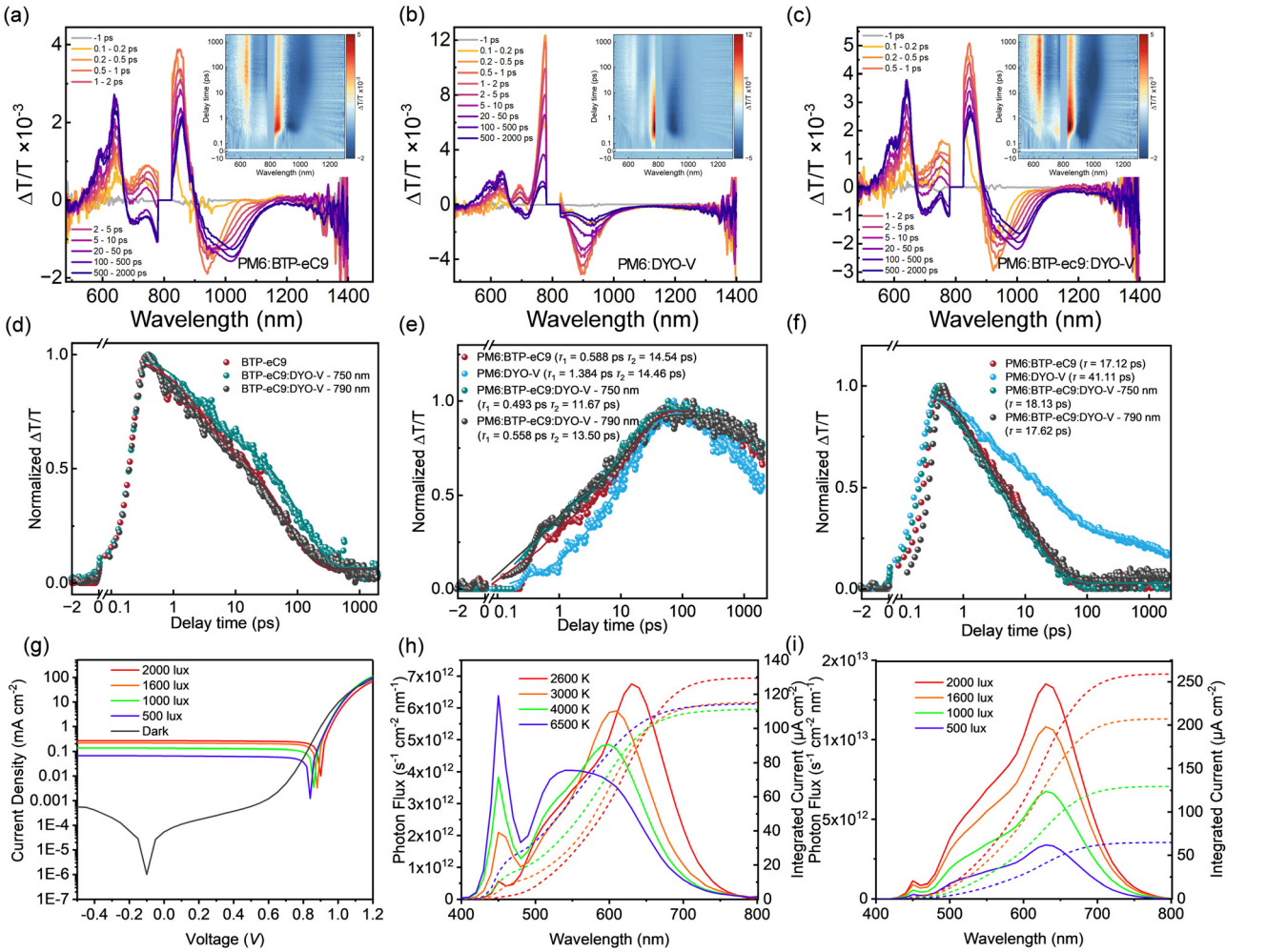

Fig. 5 TA spectroscopy of fresh PM6-blends of (a) BTP-eC9, (b) DYO-V and (c) BTP-eC9:DYO-V. (d) Time component of the local exciton (LE) component in decomposed TA spectra of fresh neat acceptor films. Time component of the (e) donor GSB and (f) delocalized exciton (DE) in decomposed TA spectra of blends with PM6. (g) Current density (log scale) as a function of voltage for PM6:DYO-V under 500, 1000, 1600 and 2000 lux and dark condition. (h) Photon flux spectrum of 2600, 3000, 4000, and 6500 K LED lamps and the integral current density of PM6:DYO-V under 1000 lux. (i) Photon flux spectrum of a 2600 K LED lamp, and the integral current density of PM6:DYO-V under light intensity conditions.

a rapid charge transfer cascade mechanism from DYO-V to BTP-eC9. Due to the lower LUMO level for BTP-eC9 compared to that of DYO-V, the transfer results in a more efficient population of the LUMO level of BTP-eC9, benefiting the photovoltaic performance.[59,60] The distinct DE state observed in the DYO-V neat films is also absent in the BTP-eC9:DYO-V neat films (Fig. S15, ESI†), further confirming the proposed mechanism. The presence of charge transfer from DYO-V to BTP-eC9 leads to a prolonged local exciton lifetime in BTP-eC9:DYO-V at 750 nm excitation (Fig. 5(d)), making the DE states formation more efficient and improving its decay (Fig. S15d, ESI†). The longer decay time of the DE state in neat acceptors indicates the suppression of non-radiative recombination processes, which clearly illustrates the positive effect from the DYO-V component on the blend's photophysical process.

Biexponential fitting of the donor GSB kinetics (Fig. 5(e)) provided the exciton dissociation (τ_1) and diffusion times (τ_2) (Table S7, ESI†).[61,62] PM6:BTP-eC9:DYO-V exhibits both faster exciton dissociation time (τ_2 = 0.558 ps) and exciton diffusion time (τ_2 = 13.50 ps), compared to PM6:BTP-eC9 (τ_1 = 0.588 ps and τ_2 = 14.54 ps), indicating a more effective hole transfer in the ternary blends. This is primarily attributed to the fast charge transfer cascade from DYO-V to BTP-eC9, thus resulting in a higher exciton dissociation efficiency. In contrast, PM6:DYO-V shows a slower hole transfer (τ_1 = 1.384 ps, τ_2 = 14.46 ps), which is consistent with the inferior hole mobility of PM6:DYO-V. In the DE kinetics (Fig. 5), PM6:BTP-eC9:DYO-V presents a slightly longer exciton lifetime than PM6:BTP-eC9, demonstrating a suppressed recombination process after the DYO-V introduction.

Indoor photovoltaic performance

The hypsochromic absorption of DYO-V matches well with the indoor LED light, which is suitable for indoor photovoltaic applications.[63] The indoor photovoltaic performance of PM6:DYO-V was evaluated using various LED light sources with different correlated color temperatures (CCTs): 2600 K, 3000 K, 4000 K, and 6500 K, representing different LED light scenarios (Fig. S16 and Table S8, ESI†). Fig. 5(g)–(i) illustrates the photon flux of the LED at different CCTs and the corresponding integral current density of the devices. Among these, 2600 K LED was identified as the optimal light source. This is due to its emission spectrum demonstrating the best overlap with PM6:DYO-V's photon absorption. Input power measurements and indoor PCE calculations were carried out in accordance with the methodology detailed in our previous work.[43] The device's performance was further accessed under varying illumination intensities (2000, 1600, 1000, and 500 lux) provided by the 2600 K LED lamp (Fig. 5(i)), corresponding to the indoor photovoltaic parameters summarized in Table 2. Remarkably, PM6:DYO-V achieved a champion PCE of 28.1% under a luminous intensity of 2000 lux, setting a new record efficiency for DGA-based indoor organic photovoltaics. Under typical working conditions (500 lux), the system demonstrated a respectable PCE of 24.9%, which is attributed to its low leakage current and is the lowest PCE value (Fig. 5(g)) observed in indoor photovoltaic systems. These results highlight the exceptional potential of developing DGA-based indoor organic photovoltaics for microelectronic devices in IoTs.

Table 2 Photovoltaic parameters of PM6:DYO-V under 2600 K LED illumination

Active layer	Light intensity [lux]	P_{in} [mW cm^{-2}]	V_{OC} [V]	J_{SC}/J_{cal} [μA cm^{-2}]	FF [%]	PCE [%]
PM6:DYO-V	500	0.159	0.841	66.0/64.7	71.5	24.9
	1000	0.318	0.861	133.1/129.4	73.5	26.5
	1600	0.509	0.879	214.6/207.1	75.2	27.9
	2000	0.637	0.898	265.6/258.9	75.1	28.1

Conclusions

In conclusion, a high-performance DGA, DYO-V, is successfully developed by incorporating alkoxy side chains on Y-series skeletons and connected by vinylene linkers. The alkoxy chain effectively blue-shifts the UV-Vis absorption and upshifts the energy levels, which leads to complementary absorption and suppressed voltage loss in the host binary device. The following PM6:BTP-eC9:DYO-V ternary OSCs achieved a significantly improved efficiency of 20.2% with a higher V_{OC} of 0.90 V and robust device stability (T_{90} = 2000 h). These properties are much better than that of the binary PM6:BTP-eC9. Throughout the systematic characterization, the improved ternary device efficiency and stability were found to benefit from the complementary light-harvesting, decreased voltage loss, superior photo dynamics process and suppressed morphology diffusion rate. Moreover, with the potential of hypsochromic DYO-V in indoor photovoltaics, the binary PM6:DYO-V achieves an efficiency of 28.1%. This work highlights the effectiveness of alkoxy substitution on DGA for tuning the optoelectrical properties and morphology stability, providing a critical advancement in balancing device efficiencies and stability, and paving the way for the commercialization of OSCs in a versatile photovoltaic application.

Data availability

The data supporting this article have been included as part of the ESI.† The *J–V* data and EQE data of the champion devices are included in *J–V* Data. xlsx and EQE. xlsx, respectively.

Conflicts of interest

There are no conflicts to declare.

Acknowledgements

H. Yu appreciates the support from the Hong Kong Research Grants Council (GRF project 16303024, 16310824) and the Strategic Hiring Scheme start-up fund of the Hong Kong Polytechnic University (Project ID: P0056175; Work Programme:

1-BDDV). H. Yan appreciates the support from the National Key Research and Development Program of China (No. 2019 YFA0705900) funded by MOST, the Hong Kong Research Grants Council (Research fellow scheme RFS2021-6S05, RIF project R6021-18, CRF projectC6023-19G, GRF project 16310019, 16310020, 16309221, 16309822), Hong Kong Innovation and Technology Commission (ITCCNERC14SC01) and Foshan-HKUST (Project No. FSUST19-CAT0202), Zhongshan Municipal Bureau of Science and Technology (no. ZSST20SC02), Guangdong-Hong Kong-Macao Joint Laboratory (no. 2023B1212120003) and Tencent Xplorer Prize. W. Y. W. is grateful for the financial support from the RGC Senior Research Fellowship Scheme (SRFS2021-5S01), Research Institute for Smart Energy (CDAQ), Research Centre for Organic Electronics (CE0P), Research Centre for Carbon-Strategic Catalysis (CE2L) and Miss Clarea Au for the Endowed Professorship in Energy (847S) and Research Centre for Carbon-Strategic Catalysis (CE2L and CE01).

References

1 J. Yi, G. Zhang, H. Yu and H. Yan, *Nat. Rev. Mater.*, 2024, **9**, 46–62.
2 S. Chen, S. Zhu, L. Hong, W. Deng, Y. Zhang, Y. Fu, Z. Zhong, M. Dong, C. Liu, X. Lu, K. Zhang and F. Huang, *Angew. Chem., Int. Ed.*, 2024, **63**, e202318756.
3 Y. Zhang, W. Deng, C. E. Petoukhoff, X. Xia, Y. Lang, H. Xia, H. Tang, H. T. Chandran, S. Mahadevan, K. Liu, P. W. K. Fong, Y. Luo, J. Wu, S. W. Tsang, F. Laquai, H. Wu, X. Lu, Y. Yang and G. Li, *Joule*, 2024, **8**, 509–526.
4 C. Zhang, J. Song, L. Ye, X. Li, M. H. Jee, H. Y. Woo and Y. Sun, *Angew. Chem., Int. Ed.*, 2024, **63**, e202316295.
5 J. Fu, Q. Yang, P. Huang, S. Chung, K. Cho, Z. Kan, H. Liu, X. Lu, Y. Lang, H. Lai, F. He, P. W. K. Fong, S. Lu, Y. Yang, Z. Xiao and G. Li, *Nat. Commun.*, 2024, **15**, 1830.
6 J. Song, C. Li, H. Ma, B. Han, Q. Wang, X. Wang, D. Wei, L. Bu, R. Yang, H. Yan and Y. Sun, *Adv. Mater.*, 2024, **36**, 2406922.
7 Y. Wang, K. Sun, C. Li, C. Zhao, C. Gao, L. Zhu, Q. Bai, C. Xie, P. You, J. Lv, X. Sun, H. Hu, Z. Wang, H. Hu, Z. Tang, B. He, M. Qiu, S. Li and G. Zhang, *Adv. Mater.*, 2024, **36**, 2411957.
8 Q. Fan, W. Su, S. Chen, T. Liu, W. Zhuang, R. Ma, X. Wen, Z. Yin, Z. Luo, X. Guo, L. Hou, K. Moth-Poulsen, Y. Li, Z. Zhang, C. Yang, D. Yu, H. Yan, M. Zhang and E. Wang, *Angew. Chem., Int. Ed.*, 2020, **59**, 19835–19840.
9 B. Fan, W. Gao, Y. Wang, W. Zhong, F. Lin, W. J. Li, F. Huang, K. M. Yu and A. K. Y. Jen, *ACS Energy Lett.*, 2021, **6**, 3522–3529.
10 C. Sun, J. W. Lee, C. Lee, D. Lee, S. Cho, S. K. Kwon, B. J. Kim and Y. H. Kim, *Joule*, 2023, **7**, 416–430.
11 X. Cheng, M. Li, Z. Liang, M. Gao, L. Ye and Y. Geng, *ACS Appl. Energy Mater.*, 2021, **4**, 8442–8453.
12 L. Ye, H. Hu, M. Ghasemi, T. Wang, B. A. Collins, J. H. Kim, K. Jiang, J. H. Carpenter, H. Li, Z. Li, T. McAfee, J. Zhao, X. Chen, J. L. Y. Lai, T. Ma, J. L. Bredas, H. Yan and H. Ade, *Nat. Mater.*, 2018, **17**, 253–260.
13 M. Ghasemi, N. Balar, Z. Peng, H. Hu, Y. Qin, T. Kim, J. J. Rech, M. Bidwell, W. Mask, I. McCulloch, W. You, A. Amassian, C. Risko, B. T. O'Connor and H. Ade, *Nat. Mater.*, 2021, **20**, 525–532.
14 X. Du, T. Heumueller, W. Gruber, O. Almora, A. Classen, J. Qu, F. He, T. Unruh, N. Li and C. J. Brabec, *Adv. Mater.*, 2020, **32**, 1908305.
15 Y. Qin, N. Balar, Z. Peng, A. Gadisa, I. Angunawela, A. Bagui, S. Kashani, J. Hou and H. Ade, *Joule*, 2021, **5**, 2129–2147.
16 L. Duan and A. Uddin, *Adv. Sci.*, 2020, **7**, 1903259.
17 Y. Lin and X. Zhan, *Acc. Chem. Res.*, 2016, **49**, 175–183.
18 Y. Liang, D. Zhang, Z. Wu, T. Jia, L. Lüer, H. Tang, L. Hong, J. Zhang, K. Zhang, C. J. Brabec, N. Li and F. Huang, *Nat. Energy*, 2022, **7**, 1180–1190.
19 M. Lv, Q. Wang, J. Zhang, Y. Wang, Z. G. Zhang, T. Wang, H. Zhang, K. Lu, Z. Wei and D. Deng, *Adv. Mater.*, 2024, **36**, 2310046.
20 F. Qi, Y. Li, R. Zhang, F. R. Lin, K. Liu, Q. Fan and A. K. Y. Jen, *Angew. Chem., Int. Ed.*, 2023, **62**, e202303066.
21 Y. Li, Z. Ge, L. Mei, H. Ma, Y. Chen, X. Wang, J. Yu, G. Lu, R. Yang, X.-K. Chen, S. Yin and Y. Sun, *Angew. Chem., Int. Ed.*, 2024, **136**, e202411044.
22 Z. Zhang, S. Yuan, T. Chen, J. Wang, Y. Q. Q. Yi, B. Zhao, M. Li, Z. Yao, C. Li, X. Wan, G. Long, B. Kan and Y. Chen, *Energy Environ. Sci.*, 2024, **17**, 5719.
23 X. Gu, Y. Wei, N. Yu, J. Qiao, Z. Han, Q. Lin, X. Han, J. Gao, C. Li, J. Zhang, X. Hao, Z. Wei, Z. Tang, Y. Cai, X. Zhang and H. Huang, *CCS Chem.*, 2023, **5**, 2576.
24 Y. Li, F. Qi, B. Fan, K. K. Liu, J. Yu, Y. Fu, X. Liu, Z. Wang, S. Zhang, G. Lu, X. Lu, Q. Fan, P. C. Y. Chow, W. Ma, F. R. Lin and A. K. Y. Jen, *Adv. Mater.*, 2024, **36**, e202313393.
25 Q. Ye, Z. Chen, D. Yang, W. Song, J. Zhu, S. Yang, J. Ge, F. Chen and Z. Ge, *Adv. Mater.*, 2023, **35**, 2305562.
26 J. Wan, T. Wang, R. Sun, X. Wu, S. Wang, M. Zhang and J. Min, *Adv. Mater.*, 2023, **35**, 2302592.
27 F. Yi, M. Xiao, Y. Meng, H. Bai, W. Su, W. Gao, Z. F. Yao, G. Qi, Z. Liang, C. Jin, L. Tang, R. Zhang, L. Yan, Y. Liu, W. Zhu, W. Ma and Q. Fan, *Angew. Chem., Int. Ed.*, 2024, **63**, e202319295.
28 S. You, Y. Zhang, B. Huang, S. Y. Jeong, X. Shuai, S. Huang, H. Y. Woo, F. Wu and L. Chen, *Adv. Funct. Mater.*, 2024, 2414803.
29 B. Fan, H. Gao, L. Yu, R. Li, L. Wang, W. Zhong, Y. Wang, W. Jiang, H. Fu, T. Chen, B. Kan, S.-W. Tsang and A. K.-Y. Jen, *Angew. Chem., Int. Ed.*, 2024, e202418439.
30 Y. Chen, F. Bai, Z. Peng, L. Zhu, J. Zhang, X. Zou, Y. Qin, H. K. Kim, J. Yuan, L.-K. Ma, J. Zhang, H. Yu, P. C. Y. Chow, F. Huang, Y. Zou, H. Ade, F. Liu and H. Yan, *Adv. Energy Mater.*, 2021, **11**, 2003141.
31 C. Wang, X. Ma, D. Deng, H. Zhang, R. Sun, J. Zhang, L. Zhang, M. Wu, J. Min, Z. G. Zhang and Z. Wei, *Nat. Commun.*, 2024, **15**, 8494.
32 Y. Li, F. Qi, B. Fan, K. K. Liu, J. Yu, Y. Fu, X. Liu, Z. Wang, S. Zhang, G. Lu, X. Lu, Q. Fan, P. C. Y. Chow, W. Ma, F. R. Lin and A. K. Y. Jen, *Adv. Mater.*, 2024, **36**, 2313393.
33 Z. Li, Z. Zhang, H. Chen, Y. Zhang, Y. Q. Q. Yi, Z. Liang, B. Zhao, M. Li, C. Li, Z. Yao, X. Wan, B. Kan and Y. Chen, *Adv. Energy Mater.*, 2023, **13**, 2300301.

34 H. M. Ng, C. H. Kwok, Z. Qi, Z. Wang, L. Chen, W. Liu, W. Zhao, H. Ade, C. Zhang, H. Yan and H. Yu, *J. Mater. Chem. A*, 2023, **11**, 22769–22774.
35 Y. Chen, T. Liu, L.-K. Ma, W. Xue, R. Ma, J. Zhang, C. Ma, H. K. Kim, H. Yu, F. Bai, B. Kam, S. Wong, W. Ma, H. Yan and Y. Zou, *J. Mater. Chem. A*, 2021, **9**, 7481–7490.
36 J. Liang, M. Pan, Z. Wang, J. Zhang, F. Bai, R. Ma, L. Ding, Y. Chen, X. Li, H. Ade and H. Yan, *Chem. Mater.*, 2022, **34**, 2059–2068.
37 H. Yu, C. Zhao, H. Hu, S. Zhu, B. Zou, T. A. Dela Pena, H. M. Ng, C. H. Kwok, J. Yi, W. Liu, M. Li, J. Wu, G. Zhang, Y. Chen and H. Yan, *Energy Environ. Sci.*, 2024, **17**, 5191.
38 L. Xie, A. Lan, Q. Gu, S. Yang, W. Song, J. Ge, R. Zhou, Z. Chen, J. Zhang, X. Zhang, D. Yang, B. Tang, T. Wu and Z. Ge, *ACS Energy Lett.*, 2023, **8**, 361–371.
39 H. Yu, Y. Wang, H. K. Kim, X. Wu, Y. Li, Z. Yao, M. Pan, X. Zou, J. Zhang, S. Chen, D. Zhao, F. Huang, X. Lu, Z. Zhu and H. Yan, *Adv. Mater.*, 2022, **34**, 2200361.
40 H. S. Ryu, S. Y. Park, T. H. Lee, J. Y. Kim and H. Y. Woo, *Nanoscale*, 2020, **12**, 5792–5804.
41 T. H. Kim, N. W. Park, M. A. Saeed, S. Y. Jeong, H. Y. Woo, J. H. Park and J. W. Shim, *Nano Energy*, 2023, **112**, 108429.
42 Y. Cui, Y. Wang, J. Bergqvist, H. Yao, Y. Xu, B. Gao, C. Yang, S. Zhang, O. Inganäs, F. Gao and J. Hou, *Nat. Energy*, 2019, **4**, 768–775.
43 Y. Cui, L. Hong, T. Zhang, H. Meng, H. Yan, F. Gao and J. Hou, *Joule*, 2021, **5**, 1016–1023.
44 F. Bai, J. Zhang, A. Zeng, H. Zhao, K. Duan, H. Yu, K. Cheng, G. Chai, Y. Chen, J. Liang, W. Ma and H. Yan, *Joule*, 2021, **5**, 1231–1245.
45 S. Luo, F. Bai, J. Zhang, H. Zhao, I. Angunawela, X. Zou, X. Li, Z. Luo, K. Feng, H. Yu, K. S. Wong, H. Ade, W. Ma and H. Yan, *Nano Energy*, 2022, **98**, 107281.
46 D. Müller, E. Jiang, P. Rivas-Lazaro, C. Baretzky, G. Loukeris, S. Bogati, S. Paetel, S. J. C. Irvine, O. Oklobia, S. Jones, D. Lamb, A. Richter, G. Siefer, D. Lackner, H. Helmers, C. Teixeira, D. Forgács, M. Freitag, D. Bradford, Z. Shen, B. Zimmermann and U. Würfel, *ACS Appl. Energy Mater.*, 2023, **6**, 10404–10414.
47 B. Fan, W. Gao, X. Wu, X. Xia, Y. Wu, F. R. Lin, Q. Fan, X. Lu, W. J. Li, W. Ma and A. K. Y. Jen, *Nat. Commun.*, 2022, **13**, 5946.
48 C. Li, J. Zhou, J. Song, J. Xu, H. Zhang, X. Zhang, J. Guo, L. Zhu, D. Wei, G. Han, J. Min, Y. Zhang, Z. Xie, Y. Yi, H. Yan, F. Gao, F. Liu and Y. Sun, *Nat. Energy*, 2021, **6**, 605.
49 C. Bannwarth, S. Ehlert and S. Grimme, *J. Chem. Theory Comput.*, 2019, **15**, 1652–1671.
50 F. Weigend, *Phys. Chem. Chem. Phys.*, 2006, **8**, 1057–1065.
51 F. Weigend and R. Ahlrichs, *Phys. Chem. Chem. Phys.*, 2005, **7**, 3297–3305.
52 S. Grimme, S. Ehrlich and L. Goerigk, *J. Comput. Chem.*, 2011, **32**, 1456–1465.
53 Y. Shi, Y. Chang, K. Lu, Z. Chen, J. Zhang, Y. Yan, D. Qiu, Y. Liu, M. A. Adil, W. Ma, X. Hao, L. Zhu and Z. Wei, *Nat. Commun.*, 2022, **13**, 3256.
54 H. Hu, M. Ghasemi, Z. Peng, J. Zhang, J. J. Rech, W. You, H. Yan and H. Ade, *Adv. Mater.*, 2020, **32**, 2005348.
55 S. E. Root, M. A. Alkhadra, D. Rodriquez, A. D. Printz and D. J. Lipomi, *Chem. Mater.*, 2017, **29**, 2646–2654.
56 D. Li, X. Zhang, D. Liu and T. Wang, *J. Mater. Chem. A*, 2020, **8**, 15607–15619.
57 Y. Fu, L. Xu, Y. Li, E. J. Yang, Y. Guo, G. Cai, P. F. Chan, Y. Ke, C.-J. Su, U.-S. Jeng, P. C. Y. Chow, J.-S. Kim, M.-C. Tang and X. Lu, *Energy Environ. Sci.*, 2024, **17**, 8893.
58 L. Chen, C. Zhao, H. Yu, A. Sergeev, L. Zhu, K. Ding, Y. Fu, H. M. Ng, C. H. Kwok, X. Zou, J. Yi, X. Lu, K. S. Wong, H. Ade, G. Zhang and H. Yan, *Adv. Energy Mater.*, 2024, **14**, 2400285.
59 H. Yu, Y. Wang, C. H. Kwok, R. Zhou, Z. Yao, S. Mukherjee, H. Hu, Y. Fu, H. M. Ng, L. Chen, D. Zhang, D. Zhao, Z. Zheng, X. Lu, H. Yin, H. Ade, C. Zhang, Z. Zhu and H. Yan, *Joule*, 2024, **8**, 2304–2324.
60 H. Yu, Y. Wang, X. Zou, J. Yin, X. Shi, Y. Li, H. Zhao, L. Wang, H. M. Ng, B. Zou, X. Lu, K. S. Wong, W. Ma, Z. Zhu, H. Yan and S. Chen, *Nat. Commun.*, 2023, **14**, 2323.
61 W. Liu, W. Wu, A. A. Sergeev, J. Yao, Y. Fu, C. Kwok, H. M. Ng, C. Li, X. Li, S. H. Pun, H. Hu, X. Lu, K. S. Wong, Y. Li, H. Yan and H. Yu, *Adv. Sci.*, 2025, **12**, 2410826.
62 L. Xie, D. Qiu, X. Zeng, C. H. Kwok, Y. Wang, J. Yao, K. Ding, L. Chen, J. Yi, H. Ade, Z. Wei, W.-Y. Wong, H. Yan and H. Yu, *Sci. China Mater.*, 2025, **68**, 860–867.
63 B. Zou, H. M. Ng, H. Yu, P. Ding, J. Yao, D. Chen, S. H. Pun, H. Hu, K. Ding, R. Ma, M. Qammar, W. Liu, W. Wu, J. Y. L. Lai, C. Zhao, M. Pan, L. Guo, J. Halpert, H. Ade, G. Li and H. Yan, *Adv. Mater.*, 2024, **36**, 2405404.

